BALANCING OF A MULTI-MASS FLEXIBLE ROTOR-BEARING SYSTEM WITHOUT PHASE MEASUREMENTS

E. J. Gunter
Professor, University of Virginia
Department of Mechanical and Aerospace Engineering

H. Springer
Assistant Professor
Technical University of Vienna
Department of Mechanical Engineering

R. R. Humphris
Research Professor, University of Virginia
Department of Mechanical and Aerospace Engineering

In this paper, the dynamic characteristics of a vertical three-mass rotor-bearing system were investigated to determine the critical speeds and the stability onset speed of an experimental rotor-bearing test system in which the bearing span could be varied. The location of the observed critical speeds were compared with the values of the predicted critical speeds. The rotor planar modes were compared with the predicted values by exciting the stationary rotor system and observing the frequencies with an FFT-analyzer. In general, excellent agreement was obtained between the predicted and measured values of the critical speeds. Various balancing methods were studied in order to balance the rotor through three critical speeds. These methods included the least squares influence coefficient method of balancing, the modal method of balancing, and the three trial weight method using component modes. This paper presents the three trial weight method of multiplane balancing without the use of phase measurements. The particular rotor-bearing system tested has three critical speeds in the operating speed range. The rotor system also has extremely high amplification factors at the various critical speeds. Because of the low damping in the rotor-bearing system, considerable difficulty was encountered in accurately balancing the rotor through all modes by the conventional least squared error method due to the problems of shaft bow, accuracy of phase and amplitude measurements, speed control, and system non-linearity.

With the three trial weight method, using theoretical normal component unbalance distributions, each mode could be accurately balanced to an extremely low level even in the presence of substantial shaft bow using only one monitoring probe and no phase measurements. It was also observed that regions of self-excited whirl instability could be encountered with the vertical rotor depending upon the level of unbalance in the system. Normally the rotor first mode shape and occasionally the second one were excited (when operating the rotor over twice its second critical speed). For substantial second and third mode components of unbalance, the rotor would operate stable in the vicinity of the second and third critical speeds with no evidence of self-excited whirl motion. Upon accurate balancing of the second and third modes large amplitudes of nonsynchronous motions would be encountered when operating at over twice the rotor first critical speed. The large nonsynchronous motion did not effect the second and third mode balancing conditions, but it would cause an upset in the first mode balancing condition by creating a shaft bow due to self-excitation of the rotor first mode shape.

It has been demonstrated that very flexible rotors may be accurately balanced in multiple planes without phase measurements through several critical speeds. In addition to balancing the rotor, the rotor modal amplification factors at the various critical speeds were determined from the three trial weight balancing procedure by having a prior knowledge of the rotor undamped modes and modal masses.

INSTRUMENTATION AND FACILITIES

(1) Figure 1 represents a schematic diagram of the vertical three-mass rotor-bearing test system that was used in this study. The shaft diameter is 9.5 mm and the total shaft length is approximately 685 mm long. Figure 2 represents a schematic diagram of the instrumentation for the vertical rotor-bearing system. A central control panel makes it possible to feed the vibration signals from any of three rotor configurations into an 8-channel FM tape recorder. Digital Vector Filters may be used to analyze the vibration signals either directly, or after passing through the FM recorder for synchronous amplitude and phase or total rotor motion. One of the problems with the highly flexible rotor-bearing system with the 9.5 mm shaft diameter and the long bearing span, is the precise control of the speed. A speed control was developed so that a ramp generator signal could be input into the drive motor to give a consistent acceleration or deceleration rate. Previous experimental studies have shown that with very flexible rotor-bearing systems, the acceleration rate can have a substantial effect on the amplitude and frequency of the rotor system when passing through the rotor critical speeds (Ref. 1). In the process of performing balancing calculations by the influence coefficient method, a consistent speed ramp must be maintained if accurate balancing data is to be achieved. In the method presented here, a precise speed control is not required.

(2) With a switching unit, the rotor vibration signal can be transmitted to the Digital Vector Filters (DVF), the Minicomputer, the Digital Signal Analyzer, or the Digital Signal Processor. A new technique for balancing a multimass shaft has been developed by the Rotor Dynamics Laboratory employing the peak-hold capabilities of the FFT analyzers. Because of the difficulty of controlling the speed ramp rate, one method of

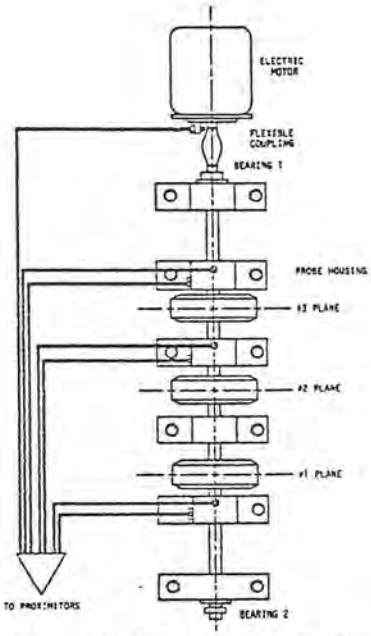

Fig. 1: Schematic Diagram of Vertical Three-Mass Rotor-Bearing System

balancing is by using the peak amplitude values as determined by the "peak-hold" capture feature of the FFT analyzer. Several oscilloscopes were used to monitor the rotor amplitudes of motion and also the vibration spectrum. A dual trace oscilloscope was used to monitor two orbits of rotor motion. These orbits could either be two separate locations along the shaft or one orbit could be the filtered or synchronous signal and the other could be the direct or total motion. The display of the rotor orbital motion on the dual beam oscilloscope was most helpful in analyzing which mode of motion was encountered and also as to whether self-excited rotor instability was occurring. From the output of the DVF, the rotor amplitude and phase could be plotted in a Bodé plot or in a polar plot on the analog plotter. Similar digital plots could also be obtained using the Minicomputer in conjunction with the Bently ADRE software and a four color pen plotter.

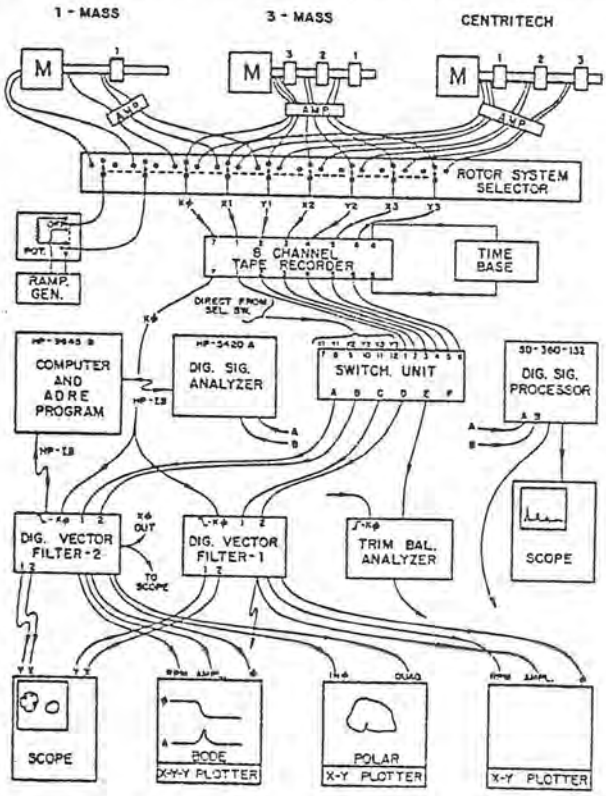

Fig. 2: Block Diagram of Experimental Equipment and Instrumentation

(3) Figure 3 represents a cross section of the vertical rotor-bearing system showing the setup of the horizontal and vertical probes at a typical shaft location. There are three mounting brackets with horizontal and vertical displacement type probes monitoring the rotor motion at three axial planes. The location of these monitoring stations may be changed, as the holes for the mounting brackets are located on 25 mm centers. The horizontal and vertical probes to monitor the shaft motion are slightly offset so as not to induce cross-coupling signals due to their close proximity. In addition to the X-Y probes to monitor the shaft motion,

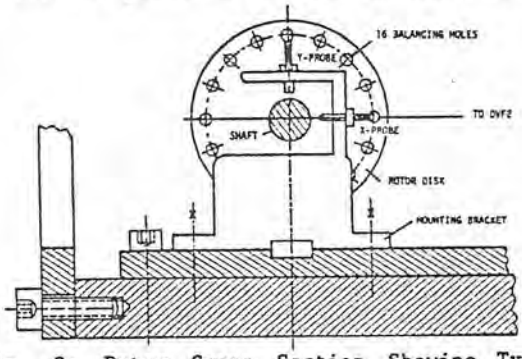

Fig. 3: Rotor Cross Section Showing Typical Probe Configuration

an additional probe called the key phasor is mounted to sense a notch on the coupling end. The key phasor probe is essential in order to trigger the DVF. If the key phasor signal is lost, then one cannot perform the rotor synchronous amplitude and phase analysis. Figure 4 represents a typical schematic diagram of the relationship between the key phasor and a vibration probe. When the timing notch passes under the key phasor, a pulse is generated. The phase angle as shown on the DVF represents the angle measured from the key phasor mark to the peak

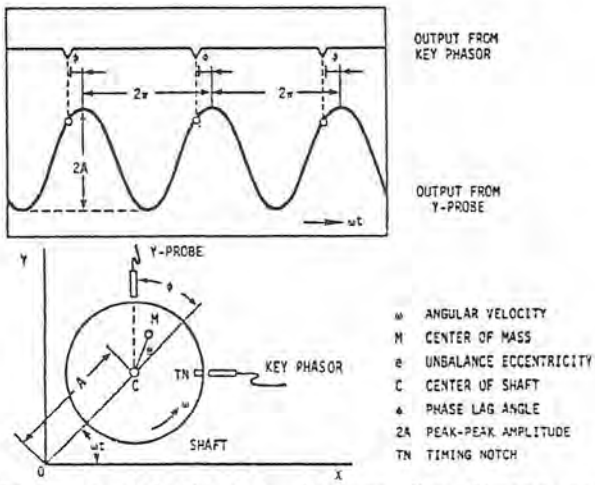

Fig. 4: Relationship Between Key Phasor and Proximity Probe Output

vibration signal of the corresponding probe being analyzed. Therefore, this angle then may be used to determine the high spot of the rotor motion. For example, if the rotor Y-motion indicates a phase angle of 45°, then one can determine the high spot of the vibrational amplitude by aligning the key phasor with the timing notch. One would then proceed to rotate 45° from the Y-probe opposite the direction of rotation. This position would determine the instantaneous high spot of the rotor vibration. Therefore, the phase angle that is observed on the DVF is a phase lag angle. The ADRE program hence treats the phase lag angle by considering this as a negative angle.

(4) Figure 5 represents typical rotor orbits observed on the oscilloscope. The inner orbit represents a synchronous orbit which is obtained by using the filtered mode on the DVF. When one employs the filtered mode, then only one timing mark is observed. If there is any nonsynchronous motion present in the system, this component will be filtered out of the motion. Therefore, when one is performing balancing calculations at high speed, extreme care must be used to insure that the rotor does not have a large self-excited instability which may cause destructive motion to the rotor-bearing system. The outer orbit in Figure 5 represents a typical nonsynchronous motion observed at high speed. Nonsynchronous components observed at low speeds normally are super-harmonic components. At low speed, it is often observed that the second and third harmonics are excited. This occurs when one is running at one-half and one-third of the rotor first critical speed. These component normally are not dangerous. When one is operating at multiples of the first critical speed however, an excitation of the rotor first critical speed may result in extremely high amplitudes of motion. Therefore, it is desirable to observe the rotor direct motion at all times.

CRITICAL SPEED ANALYSIS

In the original critical speed analysis of the vertical three-mass rotor-bearing system with 610 mm (24 in) bearing span, a 14 station model of the rotor was initially used (single-single bearing system). In the first calculation of this system, no coupling effects were assumed. The disks were also considered being integral parts of the shaft. The total mass of the computer model was 3.1 kg (6.8 lb) and the overall length 690 mm (27.2 in). A nominal bearing stiffness of 175,000 N/m (1000 lb/in) was assumed at each of both bearing locations. The first three synchronous critical speeds were predicted to be 937, 3528, and 7897 RPM. The corresponding mode shapes and the distribution of strain energy in the shaft as well as the strain energy in the bearings were calculated.

An experimental rap test was performed on the stationary rotor by lightly tapping the shaft at the center span. The resulting motion observed by the Y2-probe near the center span was analyzed by the FFT-analyzer. The first three planar frequencies were observed to be about 960, 3600, and 7800 CPM, as shown in Figure 6. The errors in the frequency prediction were 2.4%, 2.0%, and -1.2% for the first, second and third critical speeds, respectively. This result is sufficient for University research and more than accurate enough for industrial purposes.

In the preliminary testing of the vertical three-mass single-single bearing configuration, self-excited whirl instability was observed on the rotor-bearing system. This instability was determined to be primarily influenced by the lower bearing. For example, when an IRD shaft rider stick was placed in the vicinity of the lower bearing, the rotor was stabilized. Even though the bearings were centered bronze bearings with boundary lubrication, there appeared to be hydrodynamic effects generated in the rotor system which could cause self-excited whirl instability. Because of the high bearing to shaft stiffness ratio, the three-mass vertical rotor system investigated was extremely susceptible to self-excited whirl effects. A discussion of the effect of unbalance level on the onset of the stability will be presented later in this paper.

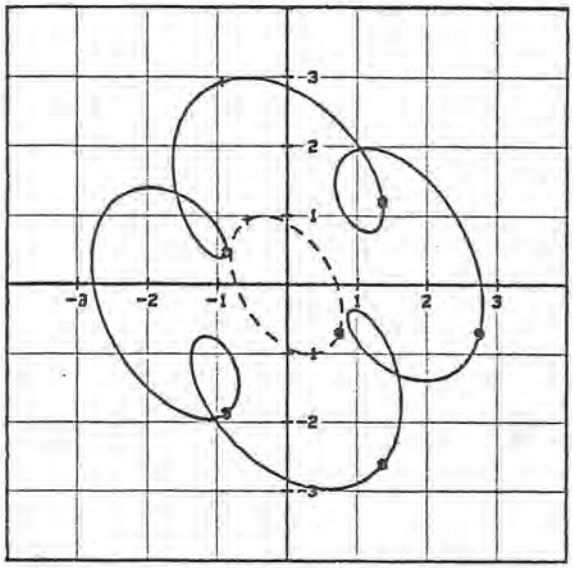

Fig. 5: Typical Rotor Orbits - Outer Loop: Nonsynchronous Orbit (direct signal of unstable rotor motion); Inner Loop: Synchronous Orbit (filtered signal).

In order to improve the stability characteristics of the rotor system, a second or dual bearing was placed at the lower bearing position. A complete set of three critical speed mode shapes was developed for the new single-

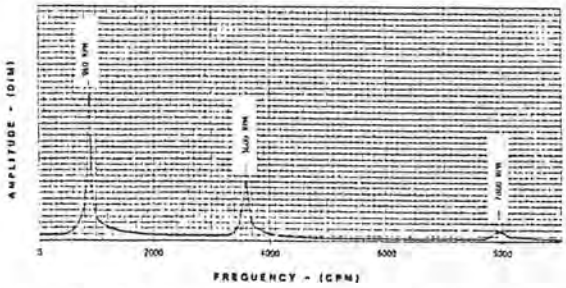

Fig. 6: Frequency Response of Impact Test on the Three-Mass Vertical Rotor, 610 mm (24") Bearing Span (Y-2 signal analyzed by an FFT analyzer, stationary rotor)

dual bearing configuration. Figure 7 represents a schematic diagram of the single-dual rotor bearing system with the 610 mm (24 in) bearing span. In this case, 17 stations were considered in the analysis and the bearing stiffness values were assumed to be 1.75 x 10^5 N/m (1,000 lb/in) at each bearing location. Figure 8 represents an animated mode shape for the first critical

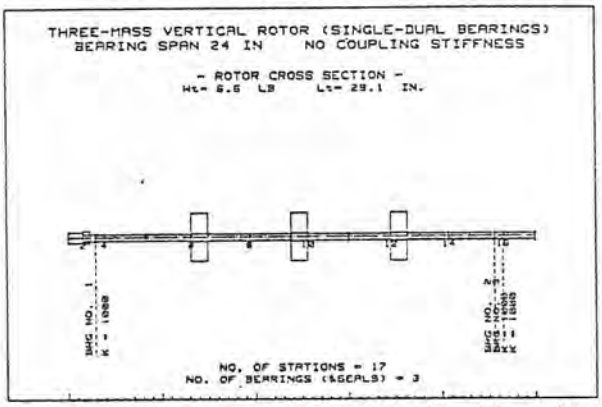

Fig. 7: Computer Model of the Three-Mass Rotor, Single-Dual Bearing System, 610 mm (24") Bearing Span

speed. In this model, the disks are not assumed to be integral with the shaft. From the observation of the mode shape, it can be seen that the third bearing is located at a nodal point and therefore does not substantially influence the first critical speed. Table 1 represents the first mode shape for the single-dual bearing system. The first critical speed was predicted to be 934 RPM. Only 7% of the total strain energy is associated with the bearing deflections. If this were to occur in an industrial turbine or compressor, it would represent a dangerous situation. Under these circumstances, the damping in the bearings is not very effective because of the low amplitude of motion at

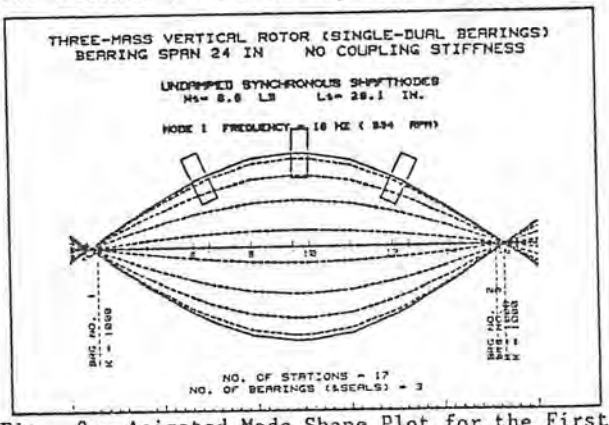

Fig. 8: Animated Mode Shape Plot for the First Critical Speed (single-dual bearing system)

the bearing locations. For example, the predicted amplitude of motion at the first bearing is only 6.3% of the maximum rotor amplitude. Therefore, the rotor first modal damping participation factor will be extremely low.

Figure 9 represents the second mode shape of the single-dual bearing system and the critical speed is predicted to be 3,567 RPM. Note, from the observation of the animated mode shape, that the maximum amplitude of motion occurs at the first and third disks. Notice that the amplitudes of these disks are approximately equal and

Table 1
Table of the First Critical Speed Mode Shape of Vertical Three-Mass Rotor, Single-Dual Bearing System, 610 mm Bearing Span, No Coupling Stiffness

UNDAMPED ROTOR MODE SHAPES AND ENERGY DISTRIBUTION
WITH TRANSVERSE SHEAR DEFORMATION
SYNCHRONOUS FORWARD MODE SHAPES

NO. 1 CRITICAL SPEED = 934 Rpm

ST	X (-)	θ (-)	M (-)	V (-)	Us (%)	Ub (%)	Kb (N/m)	Ttr (%)	Trot (%)
1	-.138	.216	0.0000	0.0000				0	0
2	-.029	.216	-.0000	-.0000				0	0
3	.063	.216	-.0000	-.0000	0	4	175E03	0	0
4	.125	.216	-.0020	-.0033				0	0
5	.423	.199	-.0120	-.0033	1			0	0
6	.703	.154	-.0229	-.0032	7			12	-0
7	.788	.142	-.0256	-.0023	2			16	0
8	.944	.076	-.0296	-.0013	15			2	0
9	1.000	.002	-.0332	-.0012	20			23	-0
10	.996	-.015	-.0331	.0001	5			23	0
11	.921	-.089	-.0289	.0014	19			2	0
12	.748	-.152	-.0244	.0015	14			13	-0
13	.659	-.163	-.0214	.0024	2			10	0
14	.395	-.202	-.0113	.0033	6			0	0
15	.063	-.217	-.0001	.0033	1	4	175E03	0	0
16	.001	-.217	-.0000	.0001	0	0	175E03	0	0
17	-.240	-.217	-.0000	.0000				0	0
					93	7		100	-0

Utotal = 53.12; Ttotal = 53.14; ERROR ENERGY BALANCE = -.0%

Modal Weight W_1 = 1.95 kg (4.3 LB)

the motions are out of phase. The center disk is at a nodal point. Therefore, radial unbalance weights located at plane 2 will have little effect on balancing the rotor second critical speed. The rotor second critical speed can best be balanced by modal weights which are equal and

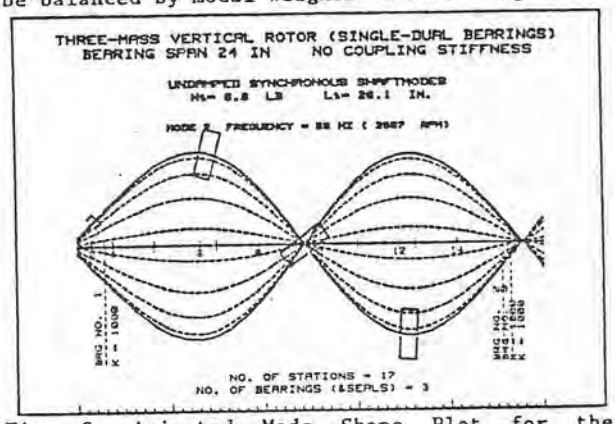

Fig. 9: Animated Mode Shape Plot for the Second Critical Speed (single-dual bearing system)

placed 180° out of phase to each other at the first and third planes. Table 2 represents the modal data for the second critical speed of the single-dual bearing system. The second mode has a total strain energy of 15% associated with the bearings. Therefore, the second mode should have a lower amplification factor than the first mode and it should be considerably easier to balance even though it will require two planes of balance correction, whereas the first mode will only require one plane of balance correction.

Figure 10 represents the animated mode shape for the third mode of the single-dual bearing system. Modal correction weights for the third mode will require three planes of balancing with the center balancing correction out of phase to the end components. The critical speed mode shape data will be used to generate these modal components, see Table 3. The strain energy distribution in the bearings for the third mode is 16%. Therefore, its modal amplification factor should be of the same order of magnitude as the

second mode and the problem of balancing the third mode should be of the same order of difficulty as balancing the second mode, except that three planes are required.

Table 4 represents the critical speed summary for the single-dual bearing system. It should be noted that the rotor modal mass is computed along with the modal moment of inertia. The modal weight, W, and modal inertia, I_t, are

Table 2
Table of the Second Critical Speed Mode Shape of Vertical Three-Mass Rotor, Single-Dual Bearing System, 610 mm Bearing Span, No Coupling Stiffness

UNDAMPED ROTOR MODE SHAPES AND ENERGY DISTRIBUTION
WITH TRANSVERSE SHEAR DEFORMATION
SYNCHRONOUS FORWARD MODE SHAPES

NO. 2 CRITICAL SPEED = 3567 Rpm

ST	X (-)	θ (-)	M (-)	V (-)	Us (%)	Ub (%)	Kb (N/m)	Ttr (%)	Trot (%)
1	.088	.309	0.0000	0.0000				0	0
2	.243	.309	.0000	.0000	0			0	0
3	.375	.309	.0002	.0002	0	10	175E03	0	0
4	.463	.307	-.0115	-.0191	0			0	0
5	.849	.211	-.0688	-.0187	3			1	0
6	1.000	-.045	-.1276	-.0174	16			25	-0
7	.956	-.109	-.1259	.0015	5			23	0
8	.621	-.336	-.0660	.0196	14			1	0
9	.065	-.418	-.0032	.0205	2			0	-1
10	-.173	-.414	.0212	.0217	0			1	0
11	-.696	-.297	.0778	.0185	4			1	0
12	-.957	-.048	.1313	.0174	16			23	-0
13	-.966	.017	.1303	-.0006	5			23	0
14	-.753	.258	.0726	-.0189	16			1	0
15	-.246	.359	.0051	-.0200	3	4	175E03	0	0
16	-.143	.360	.0004	-.0075	0	1	175E03	0	0
17	.257	.361	.0000	-.0001				0	0
					85	15		100	-0

Utotal = 722.4; Ttotal = 723.7; ERROR ENERGY BALANCE = -.2%

Modal Weight W_2 = 1.81 kg (4.0 LB)

proportional to the rotor translatory and rotary kinetic energies, respectively. If the value of I_t modal is low compared with W modal, then this indicates that the gyroscopic effects have a negligible influence on this particular mode. Note in particular, that for the first mode the I_t modal is less than 0.001 kg while W modal is 1.95 kg; therefore, the gyroscopic effect on the first mode is negligible. The first mode therefore may be treated as a single mass Jeffcott-rotor with an ideal weight of 1.95 kg and a modal stiffness of 18.56 E03 N/m. One of the important design characteristics developed by the Rotor Dynamics Laboratory is the concept of the ratio of the equivalent bearing stiffness, $K_b^* = 2K_b$, to the shaft modal stiffness, K_s. The dimensionless K-ratio for the first mode is equal to $K = K_b^*/K_s \cong 20$. This value would be unacceptable for a commercial machine. The amplification factor for the first mode for this K-value may be in the order of magnitude of Ac ≅

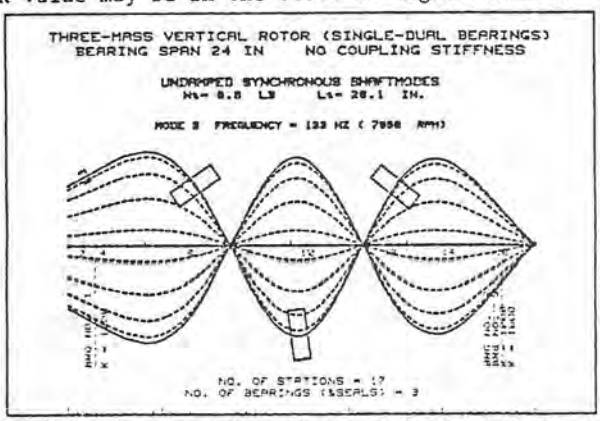

Fig. 10: Animated Mode Shape Plot for the Third Critical Speed (single-dual bearing system)

Table 3
Table of the Third Critical Speed Mode Shape of Vertical Three-Mass Rotor, Single-Dual Bearing System, 610 mm Bearing Span, No Coupling Stiffness

UNDAMPED ROTOR MODE SHAPES AND ENERGY DISTRIBUTION
WITH TRANSVERSE SHEAR DEFORMATION
SYNCHRONOUS FORWARD MODE SHAPES

NO. 3 CRITICAL SPEED = 7958 Rpm

ST	X (-)	θ (-)	M (-)	V (-)	Us (%)	Ub (%)	Kb (N/m)	Ttr (%)	Trot (%)
1	.637	.171	0.0000	0.0000				0	0
2	.723	.171	.0008	.0008				1	0
3	.796	.172	.0039	.0034	0	10	175E03	0	0
4	.845	.169	-.0183	-.0363				1	0
5	1.000	.007	-.1183	-.0326	2			2	0
6	.713	-.412	-.2023	-.0250	10			15	-1
7	.450	-.505	-.1611	.0423	3			6	0
8	-.399	-.579	.0981	.0845	2			0	0
9	-.919	-.047	.3492	.0816	19			24	-0
10	-.896	.126	.3421	-.0048	9			23	0
11	-.289	.614	.0698	-.0890	16			0	0
12	.549	.446	-.2104	-.0911	4			9	-1
13	.772	.334	-.2472	-.0395	4			17	0
14	.885	-.134	-.1465	.0331	13			2	0
15	.466	-.340	-.0120	.0399	3	3	175E03	0	0
16	.369	-.343	-.0005	.0179	0	2	175E03	0	0
17	-.012	-.343	-.0002	.0000				0	0
					84	16		101	-1

Utotal = 3,133; Ttotal = 3,147; ERROR ENERGY BALANCE = -.5%

Modal Weight W_3 = 1.59 kg (3.5 LB)

2(K+1) ≅ 42. Therefore, extremely high amplitudes of motion may be experienced at the first critical speed. Note that the modal stiffness for the second and third modes are considerably higher. The table indicates that except for the third mode, the gyroscopic effects of the rotor-bearing system should be small. Therefore, balancing should be accomplished in three planes by the N-plane procedures, as recommended by Kellenberger (Ref. 2).

Table 4
Critical Speed Summary of Vertical Three-Mass Rotor, Single-Dual Bearing System, 610 mm Bearing Span, No Coupling Stiffness

SYNCHRONOUS CRITICAL SPEED ANALYSIS WITH TRANSVERSE SHEAR DEFORMATION

Brg. NO. 1 ST. 3 Kb = 175,000 N/m
Brg. NO. 2 ST. 15 Kb = 175,000 N/m
Brg. NO. 3 ST. 16 Kb = 175,000 N/m

NO.	CRITICAL SPEED (RPM)	(HZ)	Wmode (kg)	Imode= It-(v/ω)Ip (kg)	WImode (kg)	Kmode (N/m)	Us (%)	Ub (%)	Ttr (%)	Trot (%)
1	934	16	1.95	-.000	1.95	18.56 E03	93	7	100	-0
2	3,567	59	1.82	-.009	1.81	25.34 E04	85	15	100	-0
3	7,958	133	1.60	-.014	1.59	11.02 E05	84	16	101	-1

ROTOR BALANCING BY THE THREE-TRIAL WEIGHT METHOD

Preliminary Trial Runs

A base run of the three-mass rotor was made for the various probe locations to determine the rotor amplitude response and the approximate locations of the rotor critical speeds. In the first set of runs, self-excited instability was encountered of such a magnitude that it was impossible to operate near the third critical speed. By adding a dual bearing to the lower bearing mount, the self-excited instability characteristics were greatly alleviated.

Figure 11 represents the synchronous amplitude of X1 and Y1 motion for the lower plane. This synchronous amplitude versus speed was obtained by passing the amplitude signal through the Digital Vector Filter (DVF) using the filtering mode, and then using the peak hold spectrum capabilities of the FFT Analyzer. The FFT Analyzer was calibrated by applying a test sine wave of known amplitude from a signal generator. A similar plot could have been directly obtained by connecting the Digital Vector Filter to an analog plotter. A correlation of the DVF synchronous amplitude and the peak hold spectrum

was made to determine the validity of the peak hold spectral plots obtained in this fashion. The DVF was used to condition the signal to insure that the self-excited motion, that would occasionally occur, would not be indicated as a critical speed vibration. Therefore, the peak amplitudes observed on Figure 11 represent the excitation of the rotor critical speeds as caused by unbalance in the rotor-bearing system. From this plot, it is noted that the first critical speed is 984 RPM, the second one is 3,678 RPM and the third critical speed is 7,728 RPM. The amplitude at the third critical speed in this case was the highest at 22.7 mils (576 μm). The probe locations for the lower planes are at the position where it would observe the maximum amplitude for the second critical speed. Note that the amplitude at the second critical is quite small. Therefore, the rotor is fairly well balanced for the second mode, but has a considerable amount of unbalance in the third mode component. It is of particular interest to observe the motion at the first critical speed for the X and Y probes. From careful examination of the low speed amplitude, it can be seen that the low speed motions in the X and Y probes are not identical. Under normal circumstances, shaft bow manifests itself as a uniform vector which is identical in both the X and Y-direction in bow and is 90° shifted in the phase. This effect does not appear in the three-mass vertical test rig, probably because of slight misalignment effects in the coupling and bearing anisotropic characteristics. Because of the sensitivity of the first mode, this low speed run-out difference in the two orthogonal directions caused considerable difficulty in calculating the proper magnitude of balancing for the first mode.

It is also of interest to note that for the Y1 direction of motion, a split first critical speed is observed. The Y1 direction is referred to as the local vertical direction and the X1 direction is referred to as the local horizontal direction at the first monitoring plane. In the majority of the tests performed, the local vertical Y-direction appeared to have considerably more damping than did the local horizontal X-direction. The reason for this difference may be associated with the differences in stiffness effects of the bearing support carriers, and also due to the shaft distortion caused by a misaligned coupling.

Considerations in Balancing by the Influence Coefficient and the Three-Trial Weight Method

From the observation of the rotor amplitudes of Figure 11, it is seen that the predominant amplitude of motion occurs at the third critical speed of 7,728 RPM. Note that the rotor is reasonably balanced in the first and second modes.

A well known procedure for balancing multiplane rotors is by the least squares influence coefficient method. In this procedure, a trial weight is placed in turn at the three major mass stations to be balanced. The resulting vibrations caused by the application of the trial weights over the speed range of interest lead to the generation of complex influence coefficients. In rotors of high sensitivity, the application of a single trial weight on the rotor may cause high amplitudes of motion at the lower critical speeds which prevent it from reaching full operating speed. With the least squared error procedure, a sophisticated computer program must be employed to calculate the balancing corrections. From previous experiments on a rotor system of this type with high shaft flexibility, it was difficult to balance the third mode by the least squared error method with experimental measurements of amplitude and phase near only the first two critical speeds. In order to balance the third mode accurately by the least squared error method, measurements must be made at or near the third critical speed.

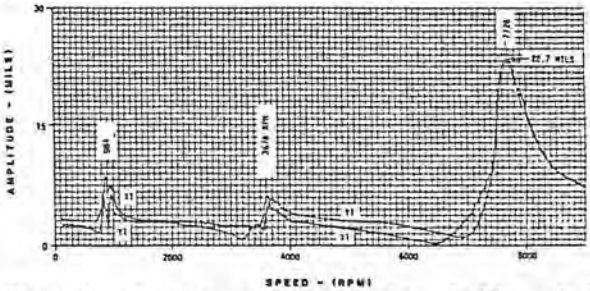

Fig. 11: Synchronous Amplitude of X1 and Y1 Motion (plane 1) of the Rotor After Balancing the First and Second Critical Speeds

The influence coefficients required by the standard least squared error technique are generated by placing individual trial unbalances along the rotor. For example, a single trial weight placed in the center plane may excite both the first and third modes. In the modal balancing procedure to be discussed in this section, a third mode balance distribution was placed on the shaft. The resulting amplitudes of motion were recorded. The modal distribution was then rotated to a new location and the procedure was repeated (three-trial weight method). Therefore, for the third mode balancing case, the number of trial runs required to generate the balancing information is no more time-consuming than the procedure required by the least squared error balancing method. In the three-trial weight procedure, no phase angle measurements are required (see Appendix). The amplitude of motion over the speed range was obtained by using the peak hold channel of the FFT Analyzer. In the absence of nonsynchronous whirl, the plot of rotor amplitude versus speed is similar to the plot obtained using the DVF on the synchronous mode. The selected amplitude of motion used in the three-trial weight method corresponded to the peak amplitude recorded at the critical speed to be balanced.

It is important to note that when using the least squared error balancing procedure, the rotor response must be measured precisely at the same speeds at which the initial amplitudes of motion are recorded. In the case of high-Λ rotors

$$\left(\Lambda = \frac{K_b L^3}{EI} = 24K = \frac{24K_b^*}{M_1 \omega_{cr1}^2} \gg 1\right) \qquad \text{(Eq. 1)}$$

which represents extremely flexible rotor bearing systems, the amplification factors at the various critical speeds are high. In order to balance accurately this class of rotor by the influence coefficient method, measurements must be taken at or near the critical speeds, par-

ticularly when the shaft has a substantial bow vector. This is often difficult to do because of the rapid shift in the phase angles encountered when passing through a critical speed with a high-Λ rotor. Therefore, in the three-trial weight modal method, the speed control is not critical. This is a practical consideration on many classes of machinery, such as induction motor drives, gas turbines, vertical feed water pumps, etc., when the speed or acceleration rate cannot be precisely controlled. It is important to note that the unbalance response for the rotor is due to both the combination of radial shaft unbalance and initial shaft bow. The complex influence coefficients, for the case of shaft unbalance and shaft bow, do not correspond at all speeds. At a critical speed, the complex influence coefficients for shaft bow and unbalance are identical (Ref. 3). Therefore, in the three-trial weight method, it is recommended that the rotor be balanced at the critical speed.

From the examination of the rotor critical speed mode shapes, see Tables 1-3, a modal distribution of unbalance weights can be approximately calculated. For a lightly damped system, a given modal unbalance distribution will excite only that corresponding mode and will be orthogonal to the other modes. Hence, it will not excite other natural frequencies in the system. The 610 mm bearing span rotor system tested has three disks located at 150 mm intervals. A slight amount of asymmetry is introduced in the system by the single-dual bearing configuration and the coupling constraint. This slight asymmetry does not substantially influence the symmetry of the modal displacements at the mass stations. The reduced modal distributions at the disk stations used in this analysis are shown in Table 5. Since the predicted critical speeds are close to the measured values, it may be assumed that the predicted undamped mode shapes are sufficiently accurate. These modes were used to develop the reduced orthogonal mode shapes as given in Table 5. Although the third mode has a small gyroscopic contribution to it, it was assumed that the rotor modal moment of inertia may be lumped with the rotor translatory vibrational mass. This assumes that all the kinetic energy of the reduced system is translatory and the reduced modes are planar.

Rotor Modal Unbalance Distributions

Any general distribution of unbalance acting on the shaft at the three major mass stations may be assumed to be resolved into three modal components, as follows (Ref. 3):

$$\{U\} = \begin{Bmatrix} U_1 \\ U_2 \\ U_3 \end{Bmatrix} = \begin{Bmatrix} U_1 \\ U_2 \\ U_3 \end{Bmatrix}_1 + \begin{Bmatrix} U_1 \\ U_2 \\ U_3 \end{Bmatrix}_2 + \begin{Bmatrix} U_1 \\ U_2 \\ U_3 \end{Bmatrix}_3 \qquad \text{(Eq. 2)}$$

Note that in general, an arbitrary unbalance located at the i'th plane will excite all three modes (unless the point is a node for a particular mode such as plane 2 for the second mode). Equation 2 can be expanded in terms of eigenvectors $\{\phi_i\}$ as

$$\{U\} = C_1\{\phi_1\} + C_2\{\phi_2\} + C_3\{\phi_3\} \qquad \text{(Eq. 3)}$$

The eigenvectors are orthogonal to each other with respect to the mass matrix.

A useful parameter is the concept of modal eccentricity E_i. For example, the unbalance distribution $\{U\}$ may be expressed as

$$\{U\} = E_1\ [M]\ \{\phi_1\} + E_2\ [M]\ \{\phi_2\} + E_3\ [M]\ \{\phi_3\} \qquad \text{(Eq. 4)}$$

Multiplying by the first mode we obtain

$$\{\phi_1\}^T\ \{U\} = E_1\ \{\phi_1\}^T\ [M]\ \{\phi_1\} + \ \ldots\ = E_1\ M_1 \qquad \text{(Eq. 5)}$$

In general,

$$E_i = \{\phi_i\}^T\ \{U\}/M_i\ , \qquad \text{(Eq. 6)}$$

where M_i is the modal mass corresponding to the i'th critical speed of the system.

Balancing the Third Mode by the Three Trial Weight Method

From Equation 6, it is desired to generate a set of trial unbalance weights such that E_1 and E_2 are zero. This, then would result in a minimal

Table 5
Rotor Modal Characteristics (Three-Mass Vertical Rotor, Single-Dual Bearing System, 610 mm Bearing Span)

Mode		1	2	3
CRITICAL SPEED (Rpm)		934	3567	7958
MODAL WEIGHT (kg)		1.95	1.81	1.59
MODE SHAPE	1	0.727	1	-0.688
	2	1	0	1
	3	0.727	-1	-0.688

excitation of the first and second modes. In the procedure for third mode balancing, a set of trial weights was chosen to be proportional to the third mode shape as given in Table 5,

$$\{U\}_{3trail} = \begin{Bmatrix} -0.34 \\ +0.50 \\ -0.34 \end{Bmatrix} \text{(grams)} \qquad \text{(Eq. 7)}$$

This trail weight distribution was applied to the rotor at a balance radius of 30 mm.

In the case of a high-Λ rotor, the application of a modal unbalance distribution placed at an arbitrary phase location on the rotor could cause catastrophic results in an actual machine which did not have accurate speed control. Although phase angles are not required in order to balance a rotor by the three-trial weight method, the knowledge of the rotor phase angles while passing through the third critical speed was utilized in order to make an initial guess as to where to first place the trial unbalance distribution. For example, the amplitude and phase angle passing through the third critical speed was observed. It was assumed approximately that the modal mass center is leading the displacement vector by 90°. Therefore, the first modal trial weight distribution in balancing the third critical was placed in hole 6,

see Figure 12. If the initial trial weight distribution were placed in holes 12-14 then permanent shaft bowing would have resulted. In the three-trial weight method, the amplitude of motion is initially measured. The measurements were taken from both the X and Y probes corresponding to the peak response observed at the third critical speed. The initial amplitude for the X2 direction was observed to be 360 μm peak to peak and 292 μm peak to peak in the Y2 direction. For example, Figure 12 represents the horizontal motion observed by the X2 probe and Figure 13 represents the vertical motion observed by the Y2 probe. It was observed that the rotor motion is not circular.

In the application of the three-trial weight method, the trial weights are applied to at least three locations and the rotor amplitudes of motion are observed at the same speed at which the initial vector is observed. For the case of third mode balancing, the rotor amplitudes of motion used in the analysis corresponded to the peak values obtained while passing through the third critical speed. These peak response values did not necessarily occur at precisely the same speed. A locus of the points drawn from the initial circle will determine the location of the unbalance and the amount. A detailed explanation of this is given in the Appendix.

A desk computer was programmed to perform the three-trial weight method balancing calculations. The listing of the computer program is given in (Ref. 6). Although this method was originally developed as a hand graphical procedure (Ref. 5,7), the application of the minicomputer represents a considerable improvement. By knowing the rotor modal mass and mode shape, the rotor modal sensitivity and modal amplification factor may also be predicted, see the Appendix. In Figure 12, the vectors Z_1 to Z_4

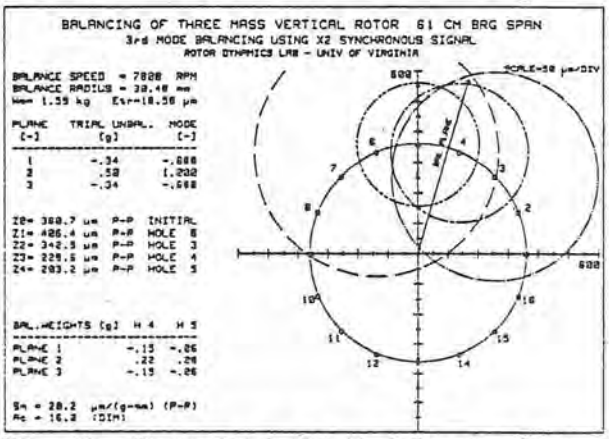

Fig. 12: Three Trial Weight Balancing Plot of X2 Motion Using the Intersection Points of Runs Z1, Z2, Z3

are drawn with the centers at the corresponding holes. For example, one can see that the smallest amplitude of motion was obtained on run 4 with the modal trial weights placed in hole 5. If the system were perfectly linear, the various circles would intersect at one point. In order to calculate the modal balancing distribution for a real system, an optimal point has to be selected by inspection from within the smallest area of intersections. This point is input into the computer via a four color pen plotter using the digitize statement. The computer then calculates the balance correction weights and a hole splitting as shown in Figure 12. It is of interest to note that the balance correction weights calculated for the vertical and horizontal planes are almost identical. However, the rotor modal sensitivity and the amplification factors for the horizontal and vertical directions are slightly different. The balance correction vector lies along the plane of the origin to the intersection point of the locus of circles. The balance correction amount is equal to the ratio of Z_o divided by Z_b and multiplied by the trial weight, see the Appendix. It is of interest to note that in the present case the balance correction weight is smaller than the initial trial weight. This accounts for the reason that in the initial run of Z_1 the application of the trial weight in hole 6 resulted in a larger amplitude of motion than the original vector Z_o. The value of Sm as shown in the bottom of Figures 12 and 13 represents the modal peak to peak sensitivity of the rotor in the third mode. Therefore, it is seen that the horizontal sensitivity for the third mode is 20.2 μm/(gmm) (p-p) modal unbalance and 16.6 μm/

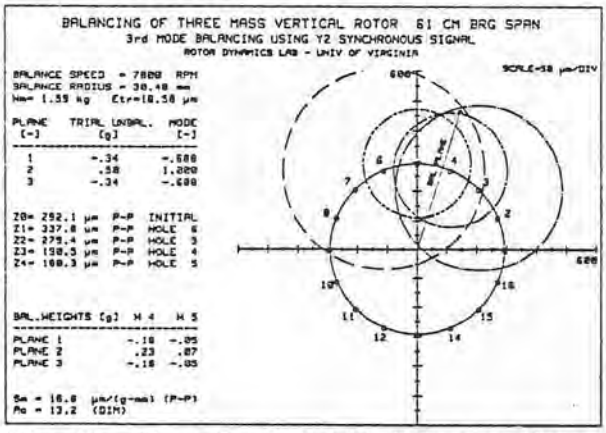

Fig. 13: Three Trial Weight Balancing Plot of Y2 Motion Using the Intersection Points of Runs Z1, Z2, Z3

(gmm) (p-p) unbalance in the vertical direction.

Another extremely important quantity calculated by this procedure is the rotor modal amplification factor. For example, the API codes for turbomachinery specify that a rotor amplification factor should not exceed the value of 8. By knowing the rotor modal mass and the rotor mode shape, the rotor modal amplification factor may be calculated. It is seen that the third modal amplification factor for the horizontal direction is 16.0 and for the vertical direction is 13.2. Therefore, it is evident that high-Λ rotors may have large amplification factors. This accounts for some of the difficulties encountered with attempting to balance with the least squared error method if speed consistency and precision are not observed in obtaining the phase angles.

From Figures 12 and 13, it is noted that the circles for the unbalance weights applied at holes 3, 4, and 5 do intersect almost at a point for both the horizontal and vertical directions. As the trial weight is moved away from the location of the balance correction, the system becomes slightly nonlinear. Therefore, this case was rerun using only the vectors Z_2 through Z_4.

The new calculations indicate that the unbalance correction has not been substantially shifted in either the amount or the location. Figure 14 represents the rotor motion at the center span for both the horizontal and the vertical directions after the third mode balancing distribution was applied to the rotor. It can be seen that the rotor is extremely well balanced for both the horizontal and vertical directions for the third mode. Of particular interest is to note that the amplitudes of motion at the first

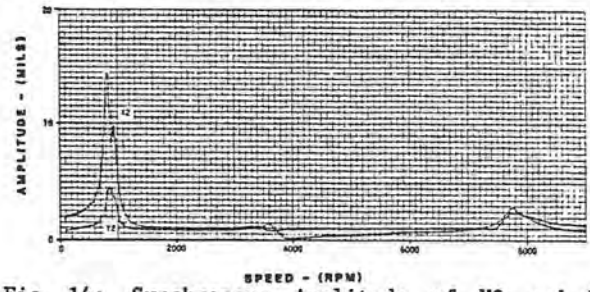

Fig. 14: Synchronous Amplitude of X2 and Y2 Motions After Balancing the Third Critical Speed

mode has increased considerably. This, however, is not necessarily due to the application of the third mode unbalance distribution.

In order to fully understand the phenomena of why the rotor amplitude of motion has increased at the first mode, a spectrum diagram or waterfall diagram was generated to show the frequency spectrum of the rotor over the entire speed range. Figure 15 represents the vibration spectrum obtained with the original rotor mounted in two bearings. This spectrum was obtained by recording the amplitude of motion over the speed range on an 8-Channel FM Tape Recorder. The rotor motion was sampled at various speeds and a spectrum analysis was made of the resulting frequencies. The spectrum was then plotted with the analog plotter. It is of importance to note that in the spectrum of the original machine, Figure 15, a small first mode excitation can be seen and a substantial third mode excitation is

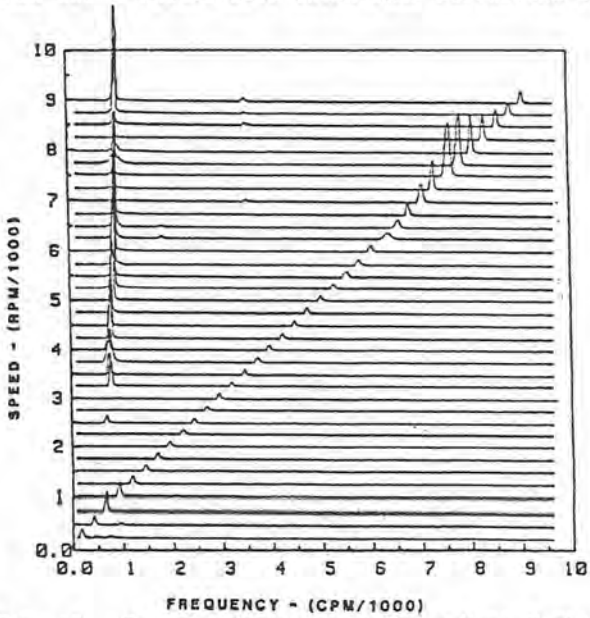

Fig. 15: Cascade Spectrum of Three-Mass Vertical Rotor, Single-Bearing System, 610 mm (24") Bearing Span - X2 Probe -200 μm/cm (20 mils/inch)

seen at ~7800 RPM. Of particular importance is to observe that at approximately 3300 RPM the rotor becomes unstable. Self-excited whirl motion is encountered in the rotor system in which the rotor first critical speed is excited. When running at 9000 RPM, the self-excited component is substantially larger than the synchronous unbalance response. It is of interest to note that the large self-excited whirl motion does not affect the third mode vibrational characteristics. However, if the rotor is run with a large amount of self-excited whirl, it will bow the rotor and will hence unbalance the first mode. Figure 15, shows also that the self-excited frequency increases slightly with operating speed. This is believed due to slight

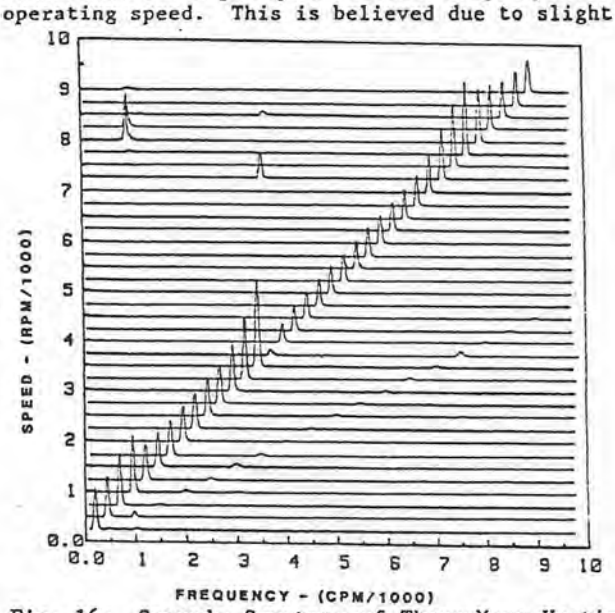

Fig. 16: Cascade Spectrum of Three-Mass Vertical Rotor, Single-Dual Bearing System, 610 mm (24") Bearing Span - X2 Probe - 200 μm/cm (20 mils/inch)

gyroscopic effects present in the first mode. In order to control the instability on the three mass experimental rotor system, a second bearing was added to form a duplex bearing at the lower bearing support. This resulted in a considerable improvement in the rotor stability characteristics, as observed in Figure 16. The self-excited whirl motion does not occur until a speed of 8000 RPM is reached. Again, it shows that the nonsynchronous motion is suppressed when the rotor is passing through the third critical speed. It is also of interest to note that a small amount of self-excited motion in the second mode was observed at 7300 RPM. This is approximately twice the rotor second critical speed.

Figure 17 represents the synchronous and direct motion taken at the horizontal center span for the original three-mass single-single bearing rotor mounted on single bearings. It can be seen that at a speed as low as 2300 RPM -- this is about twice the first critical speed -- the rotor becomes unstable as shown by the deviation of the non-synchronous or direct motion from the synchronous motion. When the rotor speed approaches the second critical, the rotor is stabilized due to the application of larger unbalance forces transmitted to the bearings. Upon passing through the second critical speed, the rotor becomes unstable again. As the rotor speed is increased, the nonsynchronous component

also increases in magnitude and reaches a maximum value of approximately 28 mils at 6500 RPM. At this speed, the nonsynchronous amplitude rapidly reduces due to the build up of the third critical speed. The nonsynchronous motion is suppressed while the rotor is passing through the third critical speed. It can be seen from

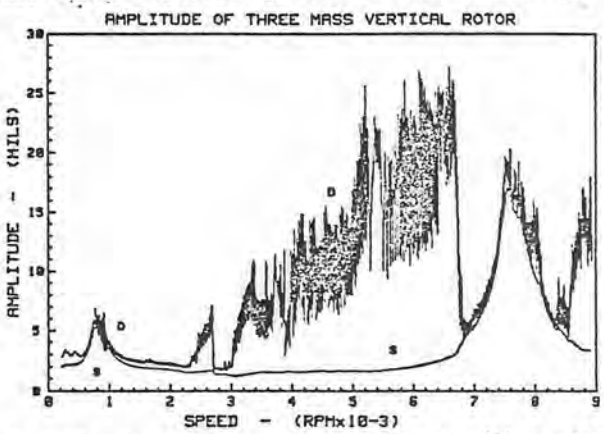

Fig. 17: Synchronous (S) and Direct (D) Amplitude of X2 Motion After Balancing the First and Second Critical Speeds. Three-Mass Vertical Rotor, (single bearing system.)

the figure that as long as the synchronous amplitude of motion is above 5 mils (125 μm) at the center span, the nonsynchronous whirl motion is suppressed. Therefore, the total motion running near the second or third critical speed with large unbalance may be paradoxically smaller than is the case for the total motion with a well balanced rotor. As the rotor passes through the third critical speed and the synchronous amplitude diminishes below 5 mils (125 μm) at a speed of 8500 RPM, the nonsynchronous motion again rapidly builds up. It is important to note that this effect of stability being controlled by the synchronous unbalance response cannot be predicted by current linear bearing theory. This effect shows the important influence of the nonlinear bearing characteristics as a function of amplitude. It also vividly illustrates the vital importance of monitoring the direct motion as well as the synchronous motion at all times.

This effect observed in the experimental three mass rotor system has also been noted on various centrifugal compressors and vertical multistage feed water pumps with axial and multi-lobed bearings. That is, some of these compressors have been operating on second critical speeds with large synchronous amplitudes. Upon balancing this particular class of machine, violent self-excited whirl developed, causing destruction to the rotor and bearings.

It was therefore concluded that the application of the third mode trial balance distribution to the experimental rotor system was not directly responsible for causing a new unbalance response at the first critical speed after the third critical had been balanced. This new first critical unbalance was indirectly caused by self-excited whirl instability creating a shaft bow.

Balancing the First Mode by the Three Trial Weight Method

The rotor first mode synchronous X2 center plane motion had a peak to peak amplitude of 15.5 mils (394 μm) before balancing as shown in Figure 18. From an examination of the vibration signal, it is estimated that the effective center shaft bow is 2.2 mils (56 μm) peak to peak and the unbalance eccentricity ($2E_1$) is 3 mils (76 μm) peak to peak and is approximately out of phase to the shaft bow. This out of phase relationship between rotor unbalance and shaft bow causes the amplitude to dip near the critical speed (Ref. 3).

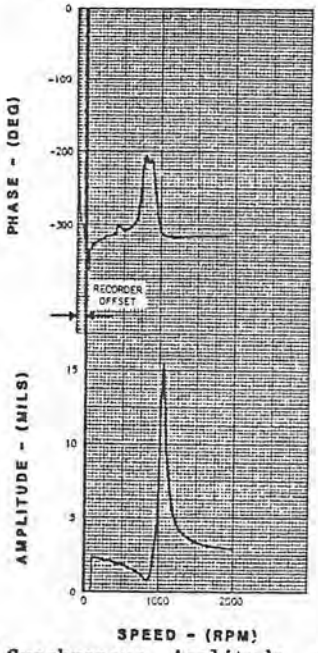

Fig. 18: Synchronous Amplitude and Phase of First Mode for X2 Motion Before Balancing

A first modal distribution of {.11 .15 .11} grams was applied to the three planes at holes 15, 2 and 13. Figure 19 represents the balancing calculations based on the X2 horizontal amplitudes of motion obtained at the first critical speed. The three runs produced a very close intersection for the prediction of the balance correction weights which are calculated to be {0.16 .22 .16} grams in planes 1 to 3 at hole 13. The modal amplification factor for the first mode for the X direction is predicted to

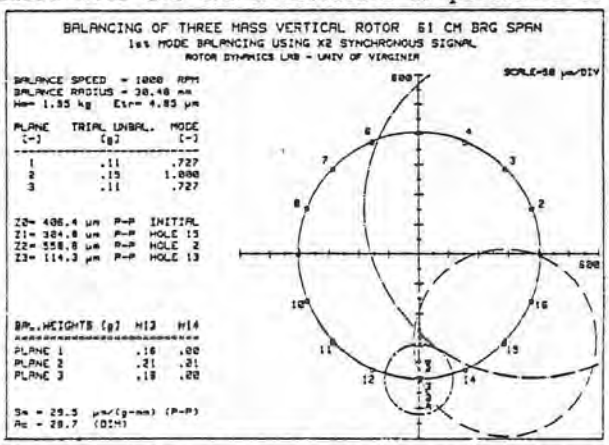

Fig. 19: Three Trial Weight Balancing Plot of X2 Motion Using the Intersection Points of Runs Z1, Z2, Z23

be 28.7.

The first mode balancing correction was also calculated using the vertical Y2-amplitudes of motion. The resulting balancing calculations are shown in Figure 20. The balancing distribution is predicted to be {.23 .32 .23} grams and split between holes 12 and 13. This balance distribution is approximately 40% larger than the predicted first mode distribution using the X2-amplitudes of motion. The phase angle balancing location using the Y2-amplitudes of motion is shifted about 15 degrees. The modal amplification factor is about half the value that was predicted for the X-direction of motion. Therefore, it is recommended that the balancing calculations be performed with both X and Y probes and that an average of the two values should be used. Normally, even for the case of anisotropic bearing stiffness and damping characteristics, the balance conditions for both the horizontal and vertical directions should be identical.

Figure 21 represents the rotor motion of the third probe station in which the rotor is balanced for the first mode in the horizontal direction. Although the rotor is well balanced in the horizontal direction, it is unbalanced in the vertical direction. The reason for this may be due to the apparent difference in the magnitude of the slow roll vectors in the X and Y directions. Normally, the absolute value of the slow roll vectors in the horizontal and vertical directions should be similar. In this case, the slow roll or shaft bow vector in the X3 direction is almost twice the magnitude of the Y3 slow roll vector. This difference in slow roll may be due to coupling constraints and misalignment. The low speed runout orbits are not synchronous, indicating coupling effects.

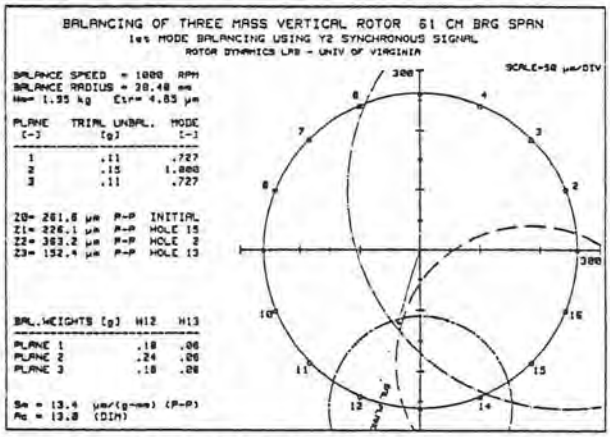

Fig. 20: Three Trial Weight Balancing Plot of Y2 Motion Using the Intersection Points of Runs Z1, Z2, Z3

The second mode also was balanced by using modal weight distributions in the first and third planes of equal weights 180 degrees out of phase. The application of the second modal unbalance distribution did not influence the rotor first mode. The second mode amplification factor was predicted to be approximately 32.

Figure 22 represents the motion at the X3 plane location after both the first and second mode balancing was applied. The balancing for these two modes is exceptionally good as the rotor

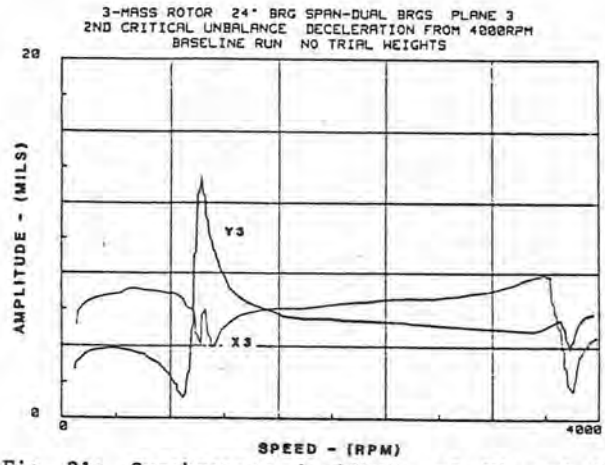

Fig. 21: Synchronous Amplitude of X3 and Y3 Motions After Balancing for First Mode in Horizontal Direction

unbalance also compensates for the shaft bow. It has not been possible with this class of rotor to achieve such a high level of balancing using the least squared error method. The reason for this difficulty is the problem of recording accurate amplitude and phase values at the selected balancing speeds. With more heavily damped systems, and with accurate speed control, the least squared error method does not suffer from such difficulties. The rapid dip in the amplitude near the first and second critical speeds is caused by the shaft bow and modal eccentricity vectors being 180° out of phase as discussed in (Ref. 3).

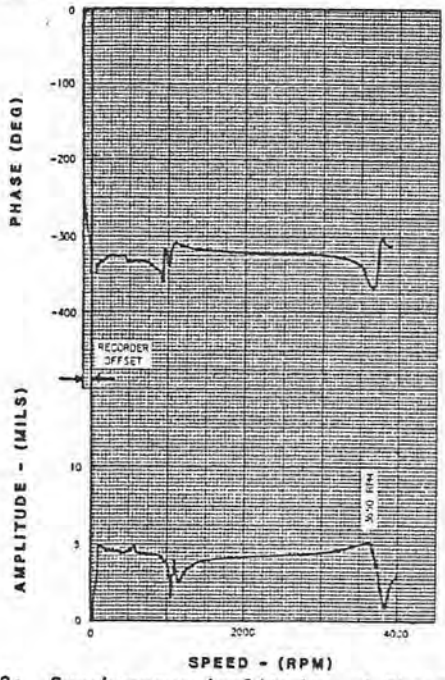

Fig. 22: Synchronous Amplitude and Phase for X3 Motion After First and Second Mode Balancing Applied

SUMMARY AND CONCLUSIONS

In this paper, it has been demonstrated that a multimass flexible rotor with shaft bow may be balanced through three critical speeds without phase measurements and using only one monitoring plane of motion. The procedure employed is a

modification of the three trial weight method using modal unbalance distributions rather than a single balancing plane. The rotor critical speeds were modeled on a minicomputer and the frequencies were compared with the experimental results obtained by exciting the rotor and analyzing the frequency spectrum with an FFT analyzer. Excellent agreement was obtained between the theoretical and experimental measurements. It is of importance to note, however, that the required mode shapes needed for the three trial weight method of balancing do not have to be precisely calculated. By knowing the rotor mode shapes, the rotor modal masses may be calculated.

In the three-mass experimental rotor analyzed, the rotor configuration is extremely flexible. There is a considerable separation of the mode shapes and frequencies. It was observed that a particular planar modal unbalance distribution did not excite the other critical speeds. The number of runs required for each modal balancing is 4. That is, the base run must be generated plus at least 3 additional runs. It is important to note that if the least squared error method is used, then 4 runs are also required to balance at 3 different planes. One of the advantages observed in the use of this method is that the rotor may be balanced even when the system exhibits nonlinear effects, such as in the bearings and in the shaft. Also, the system is not as sensitive to speed, as is the case with the influence coefficient method of balancing. By knowing the rotor modal masses, the sensitivity of each mode may be calculated. Although the three trial weight method may be performed graphically, a computer program was generated to plot the results.

For cases where it is difficult to obtain accurate phase measurements, or when the rotor speed cannot be held constant in order to take the measurements, the three trial weight method has proven to be very effective. It also has an advantage in that only one measurement plane is required. However, from a practical standpoint, several measurement planes were employed using both the horizontal and vertical directions, and balancing calculations were performed for both directions. By doing this, it demonstrated that the rotor modal amplification factor in the horizontal and vertical directions may be different. The rotor balancing predictions using the horizontal and vertical probe measurements are not identical. The reasons for this appear to be due to the differences in the rotor horizontal and vertical amplification factors caused by bearing and foundation asymmetry, and also due to the important observation that the rotor low speed runout motion is not circular. The noncircular runout may be caused by coupling misalignment. A disadvantage of this method is that the three trial weight procedure must be repeated for each mode to be balanced.

Difficulties have previously been encountered when attempting to balance extremely flexible rotors through multiple critical speeds by the least squared error method. This is because the application of a particular trial weight might excite various critical speeds in the system, limiting the operating speed of the rotor. Low speed balancing data using a least squared error procedure will not balance out the higher modes of a flexible rotor with shaft bow.

It was observed that the unbalance level in the rotor could effect the stability characteristics of the system. It was seen that as the unbalance level in the rotor diminished for the higher order modes, the rotor instability could be excited. It is therefore concluded that in the balancing of any high speed turborotor, the total motion as well as the synchronous motion should always be observed.

REFERENCES

1. Hassenpflug, H. L., Flack, R. D., and Gunter, E. J., "Experimental Study of the Critical Speed Response, of a Jeffcott Rotor with Acceleration," Journal of the Franklin Institute (July 1980), Vol. 310, No. 1, pp. 77-88.

2. Kellenberger, W., "Should a Flexible Rotor be Balanced in N or (N + 2) Planes?," Journal of Engineering for Industry, Transactions of the American Society of Mechanical Engineers (1972), Series B, Vol. 94, pp. 548-560.

3. Nicholas, J. C., Gunter, E. J., and Allaire, P. E., "Effect of Residual Shaft Bow on Unbalance Response of a Single Mass Flexible Rotor, Part I: Unbalance Response; Part II: Balancing," Journal of Engineering for Power (1976), Vol. 98, No. 2, pp. 171-181, and pp. 182-189.

4. Parkinson, A. G., Jackson, K. L., and Bishop, R. E. D., "Some Experiments on the Balancing of Small Flexible Rotors: Part I - Theory," Journal of Mechanical Engineering Science (1963), Vol. 5, No. 1, pp. 114-128.

5. Gunter, E. J., (Ed.), "Selected Papers on Field Balancing of Rotating Machinery - Advanced Theory and Techniques, Part VII," Seminar Proceedings of Vibration Institute, Clarendon Hills, Illinois (1978).

6. Gunter, E. J., Springer, H., Humphris, R. R., "Dynamic Unbalance Response and Stability Characteristics of a Vertical Three Mass Rotor-Bearing System," University of Virginia (1981), Report No. UVA/643078/MAE81/106.

7. Jackson, C., The Practical Vibration Primer, Gulf Publishing Company: Houston (1979), p. 19.

APPENDIX

Three-Trial Weight Method

The complex vector amplitude of motion at a given speed is assumed to be of the form

$$\vec{Z}(\omega) = \alpha_u(\omega)\,\vec{E} + \alpha_b(\omega)\,\vec{\delta} \qquad \text{(Eq. A1)}$$

At the critical speed, the complex influence coefficient due to shaft bow $\vec{\delta}$ and unbalance eccentricity $\vec{E}$ coincide. The modal complex amplitude at the j'th mode then is of the form

$$\vec{Z}_j = \alpha_u\Big|_{(\omega = \omega_j)} [\vec{E}_j + \vec{\delta}_j] = Z_j\, e^{i\phi_j} \qquad \text{(Eq. A2)}$$

In balancing by the three trial weight method, it is assumed that the complex vector response is a linear function of the shaft unbalance and bow effect. At a critical speed, the influence coefficients for the shaft modal unbalance and modal shaft bow are identical for lightly damped systems. The amplitude of motion then is a complex constant times the vector sum of the modal unbalance eccentricity and modal shaft bow vectors, see Figure 23.

If a trial weight or trial modal unbalance distribution is placed upon the shaft and the rotor amplitudes and phase angles are measured at the critical speed, the angle between the complex rotor amplitude and resultant vector sum of the modal unbalance eccentricity and the shaft bow will remain constant.

The three trial weight method, as illustrated in Figure 23, represents the locus of points of the response of the rotor with equal trial weight distributions placed at three different locations around the shaft. By plotting the response amplitudes Z_1 to Z_3 at the positions around the original response amplitude Z_0, a locus B of intersections is generated. The line drawn from the origin to the point B indicates the balancing plane $\vec{Z}_b$. From Figure 23 can be seen that

$$\frac{|\vec{E} + \vec{\delta}|}{Z_o} = \frac{E_{tr}}{Z_b} \quad \text{where } E_{tr} = |\vec{E}tr_i| \text{ and } Z_b = |\vec{Z}_b| \qquad \text{(Eq. A3)}$$

The amount of the initial unbalance eccentricity is then given by

$$E_b = |\vec{E} + \vec{\delta}| = \frac{Z_o}{Z_b} E_{tr} \qquad \text{(Eq. A4)}$$

The amount of the modal correction weight can be calculated by

$$W_b = W_{tr} \frac{Z_o}{Z_b} \qquad \text{(Eq. A5)}$$

where W_{tr} is the modal trial weight.

In general, it is seen that the locus of points is not an intersection but forms a triangle. It has also been observed that if large amounts of unbalance are placed on the rotor, the system response will be nonlinear. In general, however, an accurate estimation of the unbalance is given by the center of the inner section (see Figure 12 for example).

From Equation 6, the third modal unbalance eccentricity is

$$E_{b3} = \{\phi_3^T\}\ \{U_b\}/M_3 \qquad \text{(Eq. A6)}$$

The dimensionless modal amplification factor corresponding to the i'th mode can be calculated by

$$A_{ci} = Z_{oi}/2E_{bi} \qquad \text{(Eq. A7)}$$

Z_{oi} being the initial peak to peak response of the rotor at the i'th critical speed.

The modal peak to peak sensitivity of the rotor at the i'th critical speed is defined as

$$S_{mi} = Z_{oi}/(E_{bi}\ M_i) = 2A_{ci}/M_i \qquad \text{(Eq. A8)}$$

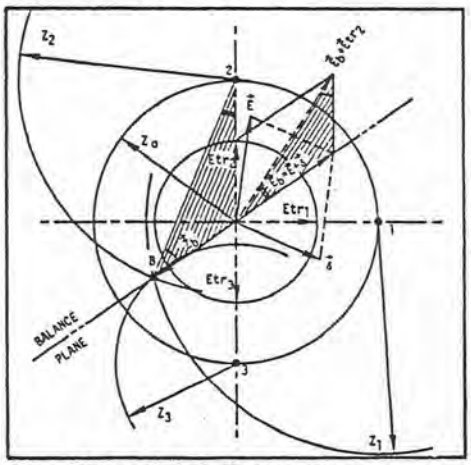

Fig. 23: Three Trial Weight Method

$\vec{E}_b$ = Initial Unbalance Eccentricity

Z_o = Initial Unbalance Response

$\vec{E}tr_1$, $\vec{E}tr_2$, $\vec{E}tr_3$ = Trial Unbalance Eccentricities

Z_1, Z_2, Z_3 = Unbalance Response Amplitudes

Example

For the third critical speed balancing, as shown in Figure 12, the balancing radius is r = 30.5 mm (1.2 inch). The modal mass from Table 5 is M_3 = 1.59 kg (3.5 lb) and the mode shape vector is $\{\phi\}_3^T = \{-0.688 \quad 1 \quad -0.688\}$.

The modal balancing weight distribution, as calculated in Figure 12, is

$$\{U_b\}/r = \begin{Bmatrix} -0.21 \\ 0.30 \\ -0.21 \end{Bmatrix} \quad \text{(gram)}$$

and the initial unbalance response Z_{o3} = 360.7 μm (peak to peak).

From Equation A6, the modal unbalance eccentricity for the third mode is calculated as

$$E_{b3} = \frac{\{-0.688 \quad 1 \quad -0.688\}}{1.59} \begin{Bmatrix} -0.21 \\ 0.30 \\ -0.21 \end{Bmatrix} \times 30.5$$

$$= 11.3 \text{ gmm/kg} = 11.3\ \mu\text{m}$$

Equations A7 and A8 yield

$$A_{c3} = \frac{Z_{03}}{2E_{b3}} = \frac{360.7}{2 \times 11.3} = 16.0$$

for the modal amplification factor and

$$S_{m3} = \frac{2A_{c3}}{M_3} = \frac{2 \times 16.0}{1.59} = 20.2\ \frac{\mu m}{gmm} = 20.2\ \frac{mils}{g\text{-}in}$$

for the modal sensitivity, as indicated at the bottom of Figure 12.